Published in final edited form as:
Cancer Res. 2017 May 01; 77(9): 2424–2438. doi:10.1158/0008-5472.CAN-15-1726.

HuR Small-Molecule Inhibitor Elicits Differential Effects in Adenomatosis Polyposis and Colorectal Carcinogenesis

Michaela Lang[1], **David Berry**[2], **Katharina Passecker**[1], **Ildiko Mesteri**[3], **Sabin Bhuju**[4], **Florian Ebner**[5], **Vitaly Sedlyarov**[5], **Rayko Evstatiev**[1], **Kyle Dammann**[1], **Alexander Loy**[2], **Orest Kuzyk**[2,†], **Pavel Kovarik**[5], **Vineeta Khare**[1], **Martin Beibel**[6], **Guglielmo Roma**[6,7], **Nicole Meisner-Kober**[6], and **Christoph Gasche**[1]

[1]Christian Doppler Laboratory for Molecular Cancer Chemoprevention, Division of Gastroenterology and Hepatology, Department of Medicine 3, Medical University of Vienna, Vienna, Austria [2]Department of Microbial Ecology, Vienna Ecology Center, Faculty of Life Sciences, University of Vienna, Vienna, Austria [3]Clinical Institute of Pathology, Medical University of Vienna, Vienna, Austria [4]Genome Analytics, Helmholtz Centre for Infection Research, Braunschweig, Germany [5]Max F. Perutz Laboratories, Center for Molecular Biology, University of Vienna, Vienna, Austria [6]Novartis Institutes for Biomedical Research, Basel, Switzerland [7]Department of Biology, University of Naples Federico II, Complesso Universitario MSA, Naples, Italy

Abstract

HuR is an RNA-binding protein implicated in immune homeostasis and various cancers, including colorectal cancer. HuR binding to AU-rich elements within the 3′ untranslated region of mRNAs encoding oncogenes, growth factors, and various cytokines leads message stability and translation. In this study, we evaluated HuR as a small-molecule target for preventing colorectal cancer in high-risk groups such as those with familial adenomatosis polyposis (FAP) or inflammatory bowel disease (IBD). In human specimens, levels of cytoplasmic HuR were increased in colonic epithelial cells from patients with IBD, IBD-cancer, FAP-adenoma, and colorectal cancer, but not in patients with IBD-dysplasia. Intraperitoneal injection of the HuR small-molecule inhibitor

Corresponding Author: Christoph Gasche, Medical University of Vienna, Waehringer Guertel 18-20, 1090 Vienna, Austria. Phone: 43-1-40400-47640; Fax: 43-1-40400-47350; christoph.gasche@meduniwien.ac.at.
†Deceased.

Disclosure of Potential Conflicts of Interest
No potential conflicts of interest were disclosed.

Authors' Contributions
Conception and design: M. Lang, P. Kovarik, G. Roma, N. Meisner-Kober, C. Gasche
Development of methodology: F. Ebner
Acquisition of data (provided animals, acquired and managed patients, provided facilities, etc.): M. Lang, D. Berry, K. Passecker, S. Bhuju, F. Ebner, V. Sedlyarov, G. Roma
Analysis and interpretation of data (e.g., statistical analysis, biostatistics, computational analysis): M. Lang, D. Berry, K. Passecker, I. Mesteri, R. Evstatiev, A. Loy, M. Beibel, G. Roma, N. Meisner-Kober
Writing, review, and/or revision of the manuscript: M. Lang, D. Berry, R. Evstatiev, K. Dammann, A. Loy, V. Khare, N. Meisner-Kober, C. Gasche
Administrative, technical, or material support (i.e., reporting or organizing data, constructing databases): V. Sedlyarov, O. Kuzyk, N. Meisner-Kober
Study supervision: C. Gasche

Europe PMC Funders Author Manuscripts

MS-444 in AOM/DSS mice, a model of IBD and inflammatory colon cancer, augmented DSS-induced weight loss and increased tumor multiplicity, size, and invasiveness. MS-444 treatment also abrogated tumor cell apoptosis and depleted tumor-associated eosinophils, accompanied by a decrease in IL18 and eotaxin-1. In contrast, HuR inhibition in APC^{Min} mice, a model of FAP and colon cancer, diminished the number of small intestinal tumors generated. In this setting, fecal microbiota, evaluated by 16S rRNA gene amplicon sequencing, shifted to a state of reduced bacterial diversity, with an increased representation of *Prevotella, Akkermansia*, and *Lachnospiraceae*. Taken together, our results indicate that HuR activation is an early event in FAP-adenoma but is not present in IBD-dysplasia. Furthermore, our results offer a preclinical proof of concept for HuR inhibition as an effective means of FAP chemoprevention, with caution advised in the setting of IBD.

Introduction

The HuR or ELAVL1 protein is a ubiquitously expressed RNA-binding protein (RBP) involved in mRNA stability regulation. HuR binds to a specific single-stranded motif in AU-rich elements (ARE) situated primarily in the 3′ untranslated regions of early response genes (1). It mainly stabilizes or alters translation of target mRNAs involved in cell growth and cell-cycle regulation (c-myc, c-fos, EGF, c-jun, cyclin A, B1, E, and D1), angiogenesis (VEGF, HIF-1α), metastasis (MMP-9, Snail), or inflammatory response (TNFα, IL1β, IL6, iNOS, TGFβ, COX-2, GM-CSF, IL10; refs. 2, 3).

In resting cells, HuR is mainly nuclear, whereas its cytoplasmic localization is linked to its functional activation to stabilize short-lived mRNAs. Altered HuR expression and localization has been implicated in various diseases such as inflammatory disorders and cancer [e.g., colorectal (4, 5), breast (6), gastric (7), ovarian (8), brain (9), skin (10), renal cancer (11)]. HuR cytoplasmic localization correlates with tumor grade and is a prognostic factor for poor overall survival in a number of cancers [e.g., breast cancer (6), ovarian carcinoma (8)]. In colorectal tumors, HuR expression and cytoplasmic abundance increases with malignancy, as reported for sporadic colorectal cancer (12) and familial adenomatous polyposis (FAP; ref. 5) and is significantly associated with elevated COX-2 expression (4, 13).

The role of HuR in inflammatory bowel disease (IBD), more specifically ulcerative colitis and Crohn's disease and subsequent development of colitis-associated cancer (CAC), is currently unclear. The *in vivo* relevance of mRNA stability regulation through AREs in inflammatory processes was first noticed by creation of a mouse lacking the ARE of TNFα mRNA. Mice developed chronic inflammatory arthritis and Crohn's-like IBD due to increased TNFα mRNA stability (14). ARE-dependent destabilization of the TNFα mRNA is largely mediated by the RBP tristetraprolin (TTP), leading to a faster mRNA turnover (14). Similarly, $TTP^{-/-}$ mice develop myeloid hyperplasia, erosive arthritis, dermatitis, cachexia, and conjunctivitis, whereas TNFα antibody administration has proven effective in counteracting these symptoms (15). These and other data suggest that aberrant regulation of RBPs or their respective mRNAs might be a major driver of inflammatory diseases.

Europe PMC Funders Author Manuscripts

Hence, it is conceivable that pharmacologic inhibition of HuR might be an attractive therapeutic strategy to combat inflammation-driven diseases or cancer. However, besides its role in pathologies, HuR has an essential function in various physiologic processes as well as embryonic development (16, 17). These diverse roles of the protein make it sheer impossible to predict the therapeutic outcome of an HuR-targeted therapy. In the absence of pharmacologic tools, genetic manipulation of the protein level may be considered as a surrogate approach. In this context, intestinal specific deletion of HuR in colorectal cancer models was reported to reduce small intestinal proliferation and resulted in a 3- and 2-fold decrease in tumor burden in APC^{Min} mice and AOM/DSS mice, respectively (18). In contrast, however, myeloid cell–specific deletion of HuR exacerbated chemically induced colitis and CAC, while myeloid cell–specific HuR overexpression protected mice from CAC (19). Postnatal deletion leads to atrophy of hematopoietic organs, loss of intestinal villi, enterocolitis, and death (16).

These data are indicative of a cell-type–specific influence of HuR activity on physiologic and pathologic processes, complicating the extrapolation of these results for clinical translation using a systemic inhibitor. In addition, it is increasingly noted that modulating protein levels by knockdown, knockout, overexpression or other genetic manipulation is a poor predictor for the outcome of pharmacologic interference (20). Therefore, studies with small-molecule antagonists or agonists in predictive disease models are essential to carefully assess the risks and benefits of HuR-targeted therapies.

Here, we examined HuR expression and localization in intestinal tissue from patients with IBD, dysplasia, CAC, colorectal cancer, and FAP and evaluated the effect of the small molecular weight HuR inhibitor MS-444 (21) as a therapeutic option for the treatment of colitis/CAC or colorectal cancer in AOM/DSS and APC^{Min} mice, respectively.

Materials and Methods

Human intestinal tissue samples

The analysis of human intestinal tissue (surgical and biopsy material) for this study was approved by the institutional review board of the Medical University Vienna (Vienna, Austria; EK Nr. 1354/2012). Serial 4-μm sections from archived, formalin-fixed, and paraffin-embedded intestinal tissue samples from patients with active ulcerative colitis (n = 6), Crohn's disease (n = 6), IBD-related dysplasia (n = 13), CAC (n = 13), FAP (n = 9), colorectal cancer (n = 10) and normal mucosa from colorectal cancer (n = 9), and FAP (n = 4) patients were analyzed for HuR protein expression (for details, see Supplementary Methods). All IBD patients had active disease with colonic involvement (for Crohn's).

Mice, treatment, and colonoscopy

C57BL/6J mice were treated with AOM/DSS and were biweekly intraperitoneally injected with 10 mg/kg MS-444 (21) dissolved in 10% N-methyl-2-pyrrolidone in Dulbecco's Phosphate-Buffered Saline (DPBS) without MgCl2 and CaCl2 or solvent only. C57BL/6J APC^{Min} mice were injected similarly with MS-444. Colonoscopy was performed 11 days after the fourth DSS cycle in wild-type (wt) mice and after 9 weeks of treatment in APC^{Min}

Europe PMC Funders Author Manuscripts

mice as stated previously (22). All animal experiments were performed in accordance with the Austrian and European law (BMWF-66.009/0265-II3b/2012). For details on experimental procedures and the short-term mouse models, see Supplementary Methods.

Histology and immunohistochemical analyses

Tissue sections were hematoxylin and eosin stained and analyzed for intestinal tumor number, size, and cancer stage (aberrant crypt foci, adenoma/dysplasia, *in situ* carcinoma and adenocarcinoma – here defined by a penetration of the muscularis mucosa). IHC staining and analysis was performed using antibodies against HuR, Ki-67, c-myc, CD8, NKp46, and F4/80 (for antibodies, see Supplementary Table S1) and standard staining procedures as described in Supplementary Methods.

Nuclear and cytoplasmic fractionation of intestinal tumors

The small intestine of APC^{Min} mice was rinsed with cold DPBS containing 50 mg/mL gentamycin and opened longitudinally. Dissected tumors from every mouse were pooled and digested with 2.5 mg/mL dispase, 2.5 mg/mL collagenase, 1 mg/mL DNase in DMEM at 37°C for 45 minutes, with pulse vortexing in between. The cell solution was pipetted up and down 5 times, passed through a 70-μm cell strainer, and 0.5 mmol/L EDTA in DPBS was added. Cells were spun down at 300 × *g* and 4°C for 5 minutes, washed twice with DPBS + gentamycin, incubated with cytoplasmic extraction buffer (10 mmol/L HEPES, 60 mmol/L KCl, 1 mmol/L EDTA, 1 mmol/L DTT, protease inhibitors, pH 7.6) containing 0.1% NP-40 on ice for 5 minutes, spun down, and the supernatant was collected as cytoplasmic fraction. The nuclear pellet was washed twice with cytoplasmic extraction buffer, resuspended in SDS sample buffer, and sonicated twice for 15 seconds. Equal volumes of protein solution were used for Western blotting using HuR, α-tubulin, and histone H3 antibodies (Supplementary Table S1).

Cell culture and small intestinal organoid culture

The human colorectal cancer cell lines HCT116, HT29, and RKO were obtained and characterized, using DNA profile and cytogenetic analysis, from the ATCC, and were passaged fewer than 6 months after resuscitation. Cells were cultured in Iscove's Modified Dulbecco's Medium (Gibco/Invitrogen) supplemented with 10% FBS (Biochrom) and penicillin–streptomycin solution (Gibco). The 1CT-HCEC, human diploid colonic epithelial cells (HCEC), were characterized and cultured as stated elsewhere (23). Upon reconstitution, 1CT-HCECs were characterized morphologically and expression of ZO-1 and β-catenin as epithelial cell markers was verified.

For CRISPR/Cas9 HuR knockout in Raw 264.7 macrophages gRNA (guiding sequence: CCACATGGCGGAAGACTGCA) against exon 2 within HuR gene (ENSMUST00000098950) and purified recombinant Cas9 protein with 2 nuclear localization signals were provided by VBCF Protein Technologies facility (http://www.vbcf.ac.at). Five micrograms of recombinant Cas9 protein were mixed with 12 μg of gRNA in Cas9 cleavage buffer (150 mmol/L KCl, 10 mmol/L $MgCl_2$, 0.5 mmol/L DTT, 0.1 mmol/L EDTA, 20 mmol/L HEPES, pH 7.5) and incubated for 10 minutes at room temperature to reconstitute active RNPs. Cas9 RNPs were electroporated into 1×10^6 Raw

264.7 cells using the Neon transfection system (Thermo Fisher Scientific) with 1680 V and a single pulse of 20 ms width. Two of 3 single clones derived from the electroporated culture with HuR-deletion verified by Western blot and Sanger sequencing of PCR-amplified locus (forward: CACAAGCTACCCAAAGAGTGC; reverse: CCTTCAAGAAACCTCTCAGGCT) were used for further experiments [CRISPR/Cas9 HuR ko clone (HuR^{ko}) T20.11: T-insertion at bp 269 of HuR mRNA and clone T20.8: 49 bp deletion spanning from the HuR gene start codon to the guide RNA–binding site]. A clone without detected indels was used as wild-type control (clone T20). Macrophages were cultured in DMEM (Invitrogen) supplemented with 10% FBS and penicillin–streptomycin solution. Cells were incubated at 5% CO_2, 37°C and a relative humidity of 95%.

Small intestinal organoids were isolated from C57BL/6J wt mice and maintained as described elsewhere (24). Two-hundred organoids in 50-μL Matrigel (BD Biosciences) droplets and 500-μL organoid culture medium (Supplementary Table S2) were grown in 24-well plates for 48 hours and treated with indicated concentrations of MS-444 for another 48 hours. Supernatants were collected and frozen at −80°C for subsequent cytokine analysis.

Western blotting

The MS-444 compound was dissolved in dimethyl sulfoxide (DMSO) at a stock concentration of 50 mmol/L and kept at −20°C. Cells were treated with 50–100 μmol/L MS-444 for up to 24 hours (DMSO ≤ 0.2%). Cells were rinsed with PBS and lysed in ice-cold RIPA buffer. Fifty micrograms of protein was boiled in SDS gel sample buffer, separated by SDS-PAGE and immunoblotted onto a polyvinylidene difluoride membrane. Primary antibodies were used as follows: c-myc and β-actin (Supplementary Table S1). Bands were visualized with anti-rabbit or anti-mouse IRDye-coupled antibodies and scanned on Odyssey imager (LI-COR Biosciences).

Real-time PCR

RNA was isolated from 50 μmol/L MS-444 and/or 10 ng/mL lipopolysaccharide (LPS) treated or untreated RAW 264.7 wt and HuR^{ko} macrophages using TRIzol reagent. One microgram RNA was transcribed into cDNA using High-Capacity cDNA Reverse Transcription Kit (Applied Biosystems). Quantitative real-time PCR was carried out in duplicates using Fast SYBR Green Master Mix (Applied Biosystems; 4385612) and mIL18 primers. Data were normalized to the endogenous control 36b4 (for sequences, see Supplementary Table S3). Relative expression levels of the transcripts were calculated using the comparative C_t method.

Multiplex immunoassay

Blood from AOM/DSS mice was collected via cardiac puncture under terminal anesthesia and serum was stored at −80°C. Cytokine profiling from serum, macrophages, and organoid supernatants was performed using ProcartaPlex Multiplex Immunoassay (Affymetrix) on a Bioplex 200 System (Bio-Rad Laboratories) following the manufacturer's instructions. Assessed analytes were VEGF-A, eotaxin-1/CCL11, GRO-α/CXCL1, and Th1/2/9/17/22Treg 17plex panel (Affymetrix). Measurements were carried out in duplicates.

Europe PMC Funders Author Manuscripts

Intestinal microbiota analysis

Fecal pellets were sampled from AOM/DSS–treated mice one day before the AOM injection and the day before colonoscopy, from APC^{Min} mice one day before colonoscopy from individual mice. Stool samples were shock-frozen in liquid nitrogen and stored at −80°C. DNA was extracted from fecal pellets using a phenol–chloroform protocol with bead beating (25). DNA was precipitated with 0.1 volumes 3 mol/L Na-acetate and 0.6 volumes of ice-cold isopropanol. DNA (150 ng) was subjected to a two-step PCR amplification targeting the 16S rRNA gene of most bacteria (V3-V4 regions: 341F, S-D-Bact-0341-b-S-17, 5′-CCTACGGGNGGCWGCAG-3′ and 785R, S-D-Bact-0785-a-A-21, 5′-GACTACHVGGGTATCTAATCC-3′ ref. 26). This protocol minimizes barcoded primer-associated bias and produces data that can reliably reproduce phylotype abundances (27). Both PCRs were carried out in triplicates, which were pooled after the first 25 cycles, 10 cycles were applied for the second PCR, yielding 464-bp amplicons with an 8 nt sample-specific barcode sequence added. Also these PCR products were pooled, purified with Agencourt AMPure beads (Beckman Coulter Genomics), and quantified with PicoGreen (Quant-iT Pico-Green, Invitrogen). Equimolar concentrations of barcoded amplicons were pooled and sequenced on an Illumina MiSeq instrument with v3 chemistry.

Sequence data were sorted into libraries using the 8 nt sample-specific barcode and primer using a custom-made in-house script, quality-filtered according to the Earth Microbiome Project guidelines, and paired-end reads were concatenated (28). Reads were then clustered into species-level operational taxonomic units (OTU) of 97% sequence identity, checked for chimeras using USEARCH, and taxonomically classified using the Ribosomal Database Project naive Bayesian classifier (29, 30). For all statistical analyses, the libraries, which varied in read depth (mean: 2,099; range: 358–6,061), were subsampled to 350 reads to avoid biases caused by unequal library size. To identify the statistical significance of factors affecting the microbiota composition (MS-444 treatment, AOM/DSS treatment, number of tumors), non-parametric permutational multivariate ANOVA (perMANOVA) was performed with the "vegan" package in R (31). Alpha and beta diversity metrics were also calculated with the "vegan" package. Indicator species analysis was performed using the "indicspecies" package in R (32). This analysis determines the strength of the association between an OTU and a condition and considers the relative frequency and abundance of OTUs in target versus nontarget conditions. To focus on abundant members of the microbiota, indicator OTUs were selected that (i) were significantly associated with a condition ($P < 0.05$), and (ii) were present at >2% abundance in at least one sample. Sequencing data are archived at the National Center for Biotechnology Information (NCBI) Sequence Read Archive under Accession Numbers SAMN03174430-SAMN03174434. Sequencing was performed on a MiSeq Personal Sequencer (Illumina). Detailed description of the sequencing can be found in Supplementary Methods.

Statistical analysis

Statistical analysis was performed using SPSS software version 21.0 (IBM). Tumor number, tumor burden, average tumor size/mouse in mm^2, area of c-myc–positive tumor cells, apoptotic, Ki-67^+, $CD8^+$, F4/80^+, NKp46^+ cells, eosinophils, neutrophils, white pulp mass in the spleen, and murine HuR expression were analyzed using independent-samples Mann–

Whitney *U* test. Crypt-villus length and percentage of intestinal epithelial surface structures were analyzed using independent samples *t* test. The adenocarcinoma incidence between groups was evaluated by Fisher exact χ^2 test. Body weight differences were calculated by determining the area under the weight × time curve as a summary measure and were analyzed with ANCOVA using the starting weight as a covariate. Serum cytokine levels (pg/mL) are represented as mean ± SD and analyzed using Independent samples *t* test. Subcellular localization of HuR protein in human diseases and in the acute colitis model was analyzed using ANOVA. *Post hoc* analysis was performed by Tukey-HSD. *P* values were considered statistically significant if less than 0.05 (*, $P < 0.05$; **, $P < 0.01$; ***, $P < 0.001$).

Results

HuR cytoplasmic expression is increased in IBD and CAC but not in dysplasia

HuR overexpression and increased cytoplasmic abundance has been reported for several human cancers (4, 6, 8, 12, 13). To compare the expression pattern of HuR in the context of intestinal inflammation and CAC to sporadic and familial colorectal cancer, intestinal tissue samples of diseased patients were stained for HuR protein (Fig. 1). In normal colonic tissue, we found HuR to be mainly localized in the nucleus with low expression in the cytoplasm. In active Crohn's disease and ulcerative colitis samples, nuclear HuR was unaltered while cytoplasmic HuR expression was significantly increased compared with normal mucosa. This effect was relatively similar for both diseases, however, cytoplasmic HuR in low- and high-grade dysplasias of IBD patients was nearly absent, whereas in CAC, nuclear and cytoplasmic HuR expression was highly increased. Increased cytoplasmic HuR was similarly found in FAP-adenomas and colorectal cancer. These results indicate that HuR is activated under inflammatory conditions in intestinal epithelial cells, in FAP-adenomas as well as in colorectal cancer cells. However, it does not seem to trigger tumor initiation in IBD-associated dysplasia. On the other hand, HuR activation is an early event after loss of APC in FAP-adenomas.

Evaluation of pharmacologic HuR inhibition in mouse models of inflammation-driven and familial/sporadic colorectal cancer

This discrepancy of HuR subcellular distribution during tumorigenesis of sporadic and inflammation-driven colorectal cancer and the differential effect of HuR deletion in myeloid and epithelial cells raised the question whether pharmacologic HuR inhibition, with the small molecular weight inhibitor MS-444, might be protective or harmful in disease setting. To appreciate the different etiologies of colorectal cancer development, we used AOM/DSS and APC^{Min} mice. Mice were injected intraperitoneally (i.p.), as this route of administration has been shown to be safe and effective up to 50 mg MS-444/kg body weight (33) and the drug is released slowly. A single application of MS-444 was shown to be safe up to 300 mg/kg body weight in healthy mice (data not shown). In this study, biweekly intraperitoneal injections of 10 and 25 mg/kg were used, to investigate long-term toxicity and efficacy at moderate doses. Detection of MS-444 in tissues for pharmacokinetics studies is considered difficult as the detection sensitivity is reached at tolerated doses. Radiolabeling of the compound is not straight forward as the compound is a natural product isolated from

Actinomyces sp. (21). Hence, to verify the functional inhibition of HuR upon MS-444 in intestinal tissue, a known HuR target gene, c-myc, a transcription factor highly relevant in colorectal cancer development and expressed in epithelial cells, was chosen as a biomarker.

Systemic HuR inhibition reduces c-myc expression and small intestinal proliferation

First, c-myc protein expression upon MS-444 was analyzed *in vitro* in two colorectal cancer cell lines (HT29 and RKO) and in 1CT-HCEC cells, a diploid immortalized human colonic epithelial cell line, by Western blot analysis. Indeed, MS-444 treatment reduced c-myc expression in a dose- and time-dependent manner (Fig. 2A). After 24 hours, the effect was lost. Furthermore, HuR inhibition by MS-444 decreased c-myc expression in tumors of both mouse models (Fig. 2B and C). In line, the number of Ki-67–positive small intestinal crypt cells was markedly reduced upon MS-444 treatment in AOM/DSS mice (Fig. 2D). These data suggest that HuR inhibition by MS-444 decreases the biomarker c-myc on protein level *in vitro* and in both mouse models of intestinal carcinogenesis.

HuR inhibition augments tumor susceptibility in AOM/DSS mice

Eight- to 9-week-old female C57BL/6J mice were injected with 10 mg/kg AOM intraperitoneally one week prior to the first of four DSS cycles (Fig. 3A). Simultaneously, biweekly intraperitoneal administration of 10 mg/kg MS-444 or solvent only was initiated. Two of 15 mice in the MS-444 group died prematurely and were not analyzed. MS-444 treatment augmented DSS-induced weight loss significantly compared with control mice (Supplementary Fig. S1A) despite DSS water consumption being similar between groups (Supplementary Fig. S1B). No signs of hepatic toxicity were found in MS-444–treated mice (data not shown). Eleven days after the fourth DSS cycle mice underwent colonoscopy. The number and size of tumors in the distal colon increased upon MS-444 compared with control mice ($P < 0.05$), due to more medium ($P < 0.05$) and large ($P < 0.001$) tumors (Fig. 3B and C). No change was observed for small tumors. Four days later, the mice were euthanized and the intestines were analyzed for tumor number, stage, and size. Macroscopic and microscopic signs of colonic inflammation were absent in both groups. Consistent with colonoscopy data, tumor multiplicity increased in the MS-444–treated group ($P = 0.065$; Fig. 3D and F). The number of aberrant crypt foci and low-grade dysplasias, but not *in situ* carcinomas or invasive carcinomas increased significantly. However, at least one carcinoma was found in every MS-444–treated mouse, compared with 10 of 15 control animals ($P < 0.05$; Fig. 3E, right). MS-444 treatment also increased total tumor burden ($P = 0.003$) and the average tumor size ($P = 0.006$; Fig. 3E).

HuR inhibition attenuates tumorigenesis in APC^{Min} mice

Here, we treated 5- to 6-week-old female and male APC^{Min} mice with MS-444 similar to AOM/DSS mice (Fig. 4A). One mouse in the control group and 3 of 12 mice in the MS-444 group died prematurely and were not analyzed. Weight gain was comparable between groups (Supplementary Fig. S1C). Colonoscopy (Fig. 4B) was performed after 9 weeks of treatment and revealed no difference for distal colonic tumors (Supplementary Fig. S1D). MS-444 reduced the total number of tumors ($P < 0.05$; Fig. 4C and F), by decreasing small intestinal tumors (Supplementary Fig. S1E), but had no effect on cecal and large bowel tumors (Supplementary Fig. S1F and S1G) or carcinoma incidence (Fig. 4E). MS-444

treatment did also not affect tumor burden and tumor size (Fig. 4D).These results suggest that upon loss of APC, HuR inhibition reduces tumor formation of small intestinal tumors.

Effect of MS-444 on apoptosis

HuR is implicated in the regulation of apoptosis both as a promoter of survival and an inducer of apoptosis under severe stress conditions (34). Several data suggest anti- and proapoptotic proteins as targets of HuR (e.g., Bcl-2, XIAP, Bax). Postnatal global deletion of HuR s leads to massive cell apoptosis in the small intestine (16), and AOM/DSS treatment in mice conditionally deleted for intestinal epithelial HuR (HuR^{IKO}) also results in increased apoptosis compared with $HuR^{f/f}$ mice (18). To investigate the effect of HuR inhibition on apoptosis, terminal deoxynucleotidyl transferase–mediated dUTP nick end labeling (TUNEL) staining was performed and the number of apoptotic cells was assessed in tumors of AOM/DSS and APC^{Min} mice. In AOM/DSS mice, MS-444 reduced TUNEL-positive cells by 3-fold, a finding not seen in APC^{Min} tumors (Fig. 5). Although MS-444 reduced the number of Ki-67–positive cells within crypt cells in the intestine of AOM/DSS mice, crypt-villus length increased without altering the number of crypt cells (Supplementary Fig. S2A), suggesting that inhibition of apoptosis prolongs survival of differentiated cells in the villi and may account for the increased tumor burden in these mice. In contrast, crypt-villus length in APC^{Min} mice was not altered (Supplementary Fig. S2B).

MS-444 increases cytoplasmic HuR levels in polyps of APC^{Min} mice and in an acute colitis model

Analysis of HuR subcellular distribution in small bowel tumors of APC^{Min} mice revealed an increased cytoplasmic abundance upon MS-444 treatment in APC^{Min} tumors as shown by IHC (Supplementary Fig. S2C and S2E). Elevated cytoplasmic HuR levels were further verified by analysis of nuclear and cytoplasmic fractions of APC^{Min} tumors by Western blot analysis (Supplementary Fig. S2G) in a short-term model (see Supplementary Methods). This modest but consistent increase in HuR cytoplasmic abundance was accompanied by increased HuR-CP1 levels, a cleavage product of HuR protein. We conclude that elevated cytoplasmic HuR levels upon MS-444 treatment are not correlated with tumor progression, as reported for various human cancers (4–6, 8) and that cytoplasmic HuR localization is not necessarily indicative for active HuR upon MS-444 treatment.

Despite its aggravating effect on tumor progression, MS-444 treatment had no effect on nuclear or cytoplasmic HuR expression in AOM/DSS mouse tumors, although cytoplasmic expression in general was very high (Supplementary Fig. S2D and S2F). In contrast, in an acute colitis model, in which C57BL/6J mice (5 each group) received a 3% DSS solution for 5 days and biweekly injections of 10 or 25 mg/kg MS-444, after AOM injection, HuR shifted from the nucleus to the cytoplasm with increasing MS-444 concentrations (Supplementary Fig. S3D and S3E). Mice showed severe weight loss in all treatment groups (Supplementary Fig. S3A). Four mice died prematurely in the control group and one in the 25 mg/kg MS-444 group, pointing to a protective effect of low-dose HuR inhibition under severe inflammation. Treatment with 10 mg/kg MS-444 resulted in only 9% loss of the epithelial lining, which increased to 24% upon 25 mg/kg MS-444, indicating that the lower dose of MS-444 promotes epithelial regeneration (Supplementary Fig. S3B and S3C).

Similarly to APC^{Min} mice, these findings were rather unexpected as cytoplasmic HuR is considered to be active and studies using MS-444 report of a retention of HuR in the nucleus upon MS-444 treatment ((21, 35)). However, MS-444 is known to inhibit HuR dimerization (21) and retention of its monomeric form of formerly active HuR, due to an inhibition of reimport, may explain cytoplasmic HuR increase upon MS-444 treatment *in vivo*.

HuR inhibition alters cytokine response and eosinophil count in AOM/DSS mice

Gross examination of AOM/DSS–treated intestines revealed no difference in inflammation upon MS-444 treatment, except for a slight decrease in lymphoid follicles (data not shown). To determine the effect of systemic HuR inhibition on cytokine, chemokine and growth factor profiles, sera from AOM/DSS–treated mice were analyzed using a multiplex immunoassay. From all cytokines investigated, only IL18, a cytokine important for epithelial regeneration upon injury, was reduced by about 50% ($P \leq 0.05$). A nonsignificant decrease was also found for IL22, IL23, and eotaxin-1/CCL11 (Fig. 6A).

Major producers of cytokines during inflammation and resolution of inflammation, among them IL18, are macrophages. To explore the effect of cytokine expression in LPS-activated macrophages upon MS-444 we used RAW 264.7 macrophages. In addition, we utilized CRISPR/Cas9 HuR knockout macrophages (RAW HuR^{ko}) to compare HuR deletion versus inhibition. HuR^{ko} was verified by Sanger sequencing and Western blot analysis (Supplementary Fig. S4A and S4B). Macrophages were treated with 10 ng/mL LPS and/or 50 μmol/L MS-444 for 4 hours, supernatants were collected and subjected to a multiplex immunoassay as performed for sera of AOM/DSS–treated mice. Among other cytokines such as IL6, IL12p70, and IL13 (Supplementary Fig. S4C), LPS-induced IL18 protein expression was reduced by 2.5-fold in wt RAW cells upon MS-444 treatment, which only had little effect on HuR^{ko} macrophages (Fig. 6B). On a mRNA level, MS-444 decreased LPS-induced IL18 expression. In contrast, HuR^{ko} macrophages were not responsive to LPS-induced increase in IL18 mRNA (Fig. 6C).

To investigate whether reduced IL18 levels in sera of AOM/DSS mice is a cause of altered immune cell number rather than mRNA stability regulation within immune cells, tumor-infiltrating immune cells, such as $F4/80^+$ macrophages, $CD8^+$ CTLs, $NKp46^+$ natural killer cells, neutrophils, and eosinophils, were analyzed in tumors from both mouse models. In AOM/DSS–treated mice, natural killer cell, macrophage, cytotoxic T cell, and neutrophil numbers were unchanged (Supplementary Fig. S5A, S5C and S5E; Fig. 6D, bottom panel). However, a considerable loss of tumor-infiltrating eosinophils was observed (Fig. 6D and F). This is in line with reduced serum eotaxin-1, which is the most important cytokine for eosinophil recruitment (36), in MS-444–treated AOM/DSS mice (Fig. 6A).

To assess a possible involvement of intestinal epithelial cells for altered cytokine/growth factor expression, small intestinal organoids were treated with 10 and 50 μmol/L MS-444 and supernatants were analyzed. MS-444 treatment decreased TNFα, IL6 and VEGF-A levels in a dose-dependent manner, all well-known mRNA targets of HuR (Supplementary Fig. S5G). IL18, IL22, IL23 and eotaxin-1 were undetectable in this experiment, pointing to a minor contribution of epithelial cells in cytokine release.

HuR inhibition alters tumor-infiltrating immune cells and spleen architecture in APC^{Min} mice

In APC^{Min} mouse tumors, MS-444 reduced CD8^{+} cytotoxic T cells, whereas no changes were observed for macrophages, natural killer cells, neutrophils, and eosinophils (Fig. 6E; Supplementary Fig. S5B, S5D and S5F). Adult APC^{Min} mice present with splenomegaly, increased splenic hematopoiesis, and lymphoid follicle depletion (37). Upon MS-444 treatment, white pulp mass increased from 8% to 12% of total spleen area and spleen weight was reduced (Supplementary Fig. S6A–S6C). The area of Peyer patches, known to be diminished in APC^{Min} mice, was increased in the MS-444–treated group, although not reaching significance (data not shown). In summary, MS-444 restored spleen architecture and Peyer patches and thereby might alter T-lymphocyte abundance.

MS-444 and microbiota

To investigate the effect of MS-444 on intestinal bacterial composition, stool samples were collected from individual mice before AOM injection (before treatment control) and one day before colonoscopy (to rule out any effect of bowel preparation). APC^{Min} mice feces were also collected before colonoscopy. Statistical analysis revealed that the composition of the intestinal microbiota of APC^{Min} mice was significantly associated with tumor numbers as well as with MS-444 treatment (perMANOVA, $P = 0.03$ and $P = 0.028$, respectively). In comparison with untreated mice, AOM/DSS treatment was associated with an altered microbiota, and so was MS-444 (perMANOVA, $P = 0.001$ and $P = 0.02$, respectively). The effect of MS-444 treatment in APC^{Min} mice was also visible in a principal coordinates analysis (PCoA), which shows how different microbiota composition is between samples (beta diversity), but not in AOM/DSS mice (Fig. 7A). Treatment of APC^{Min} mice with MS-444 led to a dramatic reduction in alpha diversity (or within-sample diversity), with reduced species-level OTU (operational taxonomic unit) richness and evenness as measured by the Simpson diversity index (Fig. 7B). Alternative measures of diversity such as the Chao1 estimated richness or the Shannon diversity index showed the same results, which was not found in AOM/DSS–treated mice (Fig. 7B; Supplementary Fig. S7A). However, the composition of the stool microbiota classified at higher taxonomic levels (by family and phylum) did not show any significant differences in abundant taxa with treatment (Supplementary Fig. S8), indicating that variation in either rare families or species-level OTU composition within abundant families was responsible for the distinctive alterations in the microbiota. Lookig at OTUs, indicator species analysis revealed OTUs that were characteristic for MS-444 treatment in APC^{Min} mice (Fig. 7C). Specifically, there was enrichment of members of the *Akkermansia, Prevotella*, and *Lachnospiraceae*, and a decrease in many OTUs including members of the *Bacteroidales, Lachnospiraceae, Clostridiaceae,* and *Rikenellaceae*. Indicator OTUs characteristic for AOM/DSS treatment in C57BL/6 mice were identified but not for additional MS-444 treatment (Supplementary Fig. S7B).

Discussion

The modification of RNA-binding proteins is considered an attractive target for immune-mediated disorders and cancer therapy. HuR is overexpressed in various human cancers, acts

on key tumor pathways (34, 38, 39), and regulates immune response (14, 40). Our data are in line with previous studies regarding the upregulation of HuR in familial and sporadic colorectal cancer and extend such to CAC. Notably, HuR is already activated in FAP adenomas (lacking APC). In colitis, however, neoplastic progression (i.e., dysplasia) was found independent of HuR activation. Such discrepancy was also observed in mice, as the low molecular weight HuR inhibitor MS-444 increased tumor burden in the AOM/DSS colitis model but reduced number of tumors in APC^{Min} mice. Loss of APC seems to be an important denominator for activation of HuR, which itself is an effector in APC-mutated tumors, such as a stabilizer of COX-2 mRNA together with β-catenin (41) or c-myc mRNA stability regulation.

Efforts have been made to dissect the tissue- and cell specific involvement of HuR via knockout and overexpression experiments. In this context, HuR myeloid cell–specific deletion aggravated tumor development upon AOM/DSS, while myeloid-specific overexpression was protective (19). In contrast, intestinal epithelial–specific deletion of HuR (HuR^{IKO}) resulted in a 2-fold decrease in tumor burden upon AOM/DSS treatment (18). Such reduction in tumor burden was even more pronounced in HuR^{IKO} APC^{Min} mice. The deletion or overexpression of a certain protein, however, does not always resemble the effects of pharmacologic interference (20). In light of these impediments, it is of substantial importance to examine the effect of pharmacologic (and potentially systemic) HuR inhibition on disease progression, which more resembles a therapeutic scenario in comparison to cell type–specific knockout of HuR. Because of sensitivity issues in detecting the parent compound and its metabolites from tissue extracts by standard methods (unpublished data), data on pharmacokinetics are still lacking. However, until such data become available, this study provides first data to enable the design of future pharmacokinetics and pharmacodynamics studies and provides a first step towards characterizing the benefits and adverse effects of small-molecule HuR inhibition in colorectal cancer disease models. Also, future studies would require more detailed toxicity profiles, evaluation of more mRNA targets modified by HuR inhibition, and different routes of administration (intravenous, oral). Alternatives to MS-444, which were shown to inhibit HuR, such as dehydromutactin and okicenone, also inhibiting HuR dimerization, or mitoxantrone, cethylpiridinium chloride, quercetin, b-40, and 15,16-dihydrotanshinone-I (DHTS), which were shown to interfere with TNFa mRNA binding, would be worth investigating to verify the divergent effect of HuR inhibition in colorectal cancer versus CAC mouse models (21, 42). In our study, intraperitoneal application of the compound has been chosen as MS-444 is metabolized fast if intravenously injected (Meisner-Kober, personal communication). A compound concentration of 10 or 25 mg/kg MS-444 has been used, as complete HuR inhibition might be detrimental and no long-term studies of HuR inhibition have been performed yet. In that context, MS-444 has been shown to inhibit myosin light-chain kinase (MLCK) *in vitro* (43). In our study, no obviously dilated jejuni nor compacted feces in the cecum of APC^{Min} mice were found, as characteristic for smooth muscle–specific MLCK knockout mice, as a result of gut dysmotility (44). Also, smooth muscle layer thickness within the jejunum and weight gain as a measure for (muscle) wasting was not different between sham- and MS-444–treated APC^{Min} mice (Supplementary Fig. S1C).

Nevertheless, we cannot rule out that a certain dysmotility of the intestine influences fecal passage and hence intestinal inflammation in AOM/DSS mice.

In the AOM/DSS mouse model, the tumor number was increased upon MS-444 treatment, with apparently bigger tumors and more invasive carcinomas. In this model, systemic HuR inhibition rather resembles the phenotype of myeloid-specific HuR deletion (19), emphasizing the importance of myeloid cells in disease progression and a potential profound effect of systemic HuR inhibition on myeloid cells (or general cells from the hematopoietic lineage), which might shield the protective effect of HuR inhibition on epithelial cells.

Cytokine profiling identified IL18 to be mostly downregulated by MS-444 in AOM/DSS mice and MS-444 reduced LPS-induced IL18 mRNA and protein level in macrophages (Fig. 6). IL18 is mainly produced by macrophages, dendritic cells, eosinophils, but also intestinal epithelial cells (45, 46). IL18 exerts a dual role in inflammation and homeostasis. On the one hand, it drives immune response by activating type 1 and type 17 helper T cells, on the other hand it increases intestinal barrier function and regeneration to protect from microbiota. Downregulation of IL18 may hence impede T-cell response to DSS injury and epithelial regeneration or proliferation in general. In line, our results from the acute DSS model point to a reduced reepithelialization at higher MS-444 concentrations (Supplementary Fig. S3B). Most remarkably, serum samples that revealed this change in IL18 production in the chronic AOM/DSS model were collected 15 days after the fourth DSS cycle at a point in time, when mice had fully recovered from DSS-induced injury without colonic signs of inflammation. This may also explain the low abundance of IL6 (9), TNFα (47), and VEGF-A (48) in the serum, which are actual HuR targets themselves and which were downregulated upon MS-444 in small intestinal organoids (Supplementary Fig. S5G). The abundance of IL18, which is not a known HuR target, and the effect of HuR inhibition on its expression indicate that the source of IL18 is rather tumor-associated immune cells (or epithelial cells) than an inflammatory response to DSS. Indeed, tumor-associated eosinophils, also capable of IL18 secretion, were found depleted upon MS-444 (Fig. 6D). Previously, it was shown that eotaxin-1, another HuR target (40) and also produced by macrophages and intestinal epithelial cells, is responsible for the recruitment of eosinophils (36). In our study, although the number of tumor macrophages was not altered, diminished eotaxin-1 serum levels were found upon MS-444. These data suggest a protective role of IL18, eotaxin-1, and eosinophils in the AOM/DSS model. HuR inhibition counteracts eosinophil recruitment into tumors and increases tumor size and invasiveness. Tumor eosinophils were also associated with metastasis-free disease and a better survival in human colorectal cancer (49).

Another potential mechanism for the increase in tumor size and invasiveness is the prolonged cell survival. Impediment of apoptosis in tumors (Fig. 5) might explain accelerated tumor growth in AOM/DSS mice upon MS-444. The question remains whether this is a direct effect of MS-444 on HuR or an off-target effect. Currently, we cannot specify the cell types upon which MS-444 is acting but assume that its block of apoptosis is a major contributor to the increase in tumor burden.

In contrast to AOM/DSS mice, MS-444 treatment in APC^{Min} mice led to a 25% reduction in (small intestinal) tumors without a change in tumor size or invasiveness (Fig. 4). This is not

surprising as HuR has been shown to control β-catenin (12) mRNA stability and translation as well as COX-2 expression through inhibition of miRNA-16 targeting (50). Our data are also in line with a reduction in tumor burden in HuR^{IKO} APC^{Min} mice (18). This makes HuR an important oncogene during colorectal carcinogenesis. Here we also show that HuR is upregulated immediately after the loss of APC both in human FAP polyps (Fig. 1) and in early mouse small intestinal tumors (Supplementary Fig. S2C and S2E).

One controversially discussed target of HuR is c-myc, acting both as translational repressor and mRNA stabilizer, depending on cell type and methodologic approach. HuR and let-7–loaded RISC-complex cooperate to repress c-myc translation, as shown for HeLa cells (38). In line, deletion of HuR (HuR^{IKO}) increased c-myc mRNA and protein level (18). In contrast, in oral cancer cells, HuR knockdown decreased c-myc mRNA levels (39). In our study, in both AOM/DSS and APC^{Min} mouse tumors, as well as *in vitro*, c-myc protein levels were reduced upon MS-444 treatment. Downregulation of c-myc protein upon HuR inhibition might contribute to reduced tumor number in APC^{Min} mice but might be negligible for intestinal homeostasis in the context of CAC. Downregulation of c-myc *in vivo* upon MS-444 in tumor epithelial cells indicates that the compound is actually reaching the target tissue and can be used as a biomarker for effective compound administration.

Most interestingly, MS-444 treatment was associated with a strong reduction in intestinal bacterial diversity in APC^{Min} mice (Fig. 7B). OTUs that characteristically increased due to treatment belonged to *Akkermansia, Prevotella*, and *Lachnospiraceae* (Fig. 7C). Members of these taxa have been associated with mucus degradation and/or associated with the mucus layer (51), which may suggest that MS-444 affects factors governing mucosal colonization. It is unlikely that MS-444 directly affects microbiota composition as it is injected intraperitoneally. The microbiota-altering effect of MS-444 may be due to changes in immune state, impaired tissue repair, and impediment of proliferation, which is probably due to reduced signaling of IL18. Indeed, IL18-deficient mice had distinct changes in the gut microbiome composition including an increase in members of the family *Prevotellaceae* (52) and a more pronounced colitis compared with wt mice. A direct relationship between decreased IL18 levels and increased *Prevotellaceae* abundance (or other microbes) still needs to be determined.

HuR is not only implicated in mRNA stability regulation of thousands of mRNAs, but has been shown by (photoactivatable ribonucleoside enhanced) crosslinking and immunoprecipitation ((PAR-)CLIP) to bind also to intronic sequences, suggesting HuR to be involved in splicing as shown in HeLa and HEK293 cells (53, 54). Furthermore, PAR-CLIP revealed miRNA-binding sites in close proximity to HuR-binding sites (53–55). Whether MS-444 administration affects intronic binding and potential splicing functions of HuR or regulation of miRNA expression is yet to be determined.

In summary, systemic administration of MS-444 alters the profile of inflammatory mediators, proliferation, and apoptosis in the two mouse models investigated, being favorable in APC^{Min} mice and deleterious in AOM/DSS mice for intestinal tumor progression (see also summary Fig. 7D). HuR inhibition as therapeutic option for patients with FAP remains promising. A thorough analysis of MS-444 pharmacokinetics and target

cells and tissues affected upon different routes of administration is still needed to fully appreciate HuR inhibition in the context of disease amelioration or progression.

Supplementary Material

Refer to Web version on PubMed Central for supplementary material.

Acknowledgments

The 1CT cells (HCEC) were a kind gift from Jerry W. Shay (Department of Cell Biology, Division of Digestive and Liver Diseases, University of Texas Southwestern Medical Center, Dallas, TX). We want to thank Friedrich Wrba (Clinical Institute of Pathology, Medical University of Vienna, Vienna, Austria) for providing human tissue samples. We want to thank V. Sigl (Institute for Molecular Biotechnology, Vienna, Austria) for teaching small intestinal organoid isolation, and Margarete Focke-Tejkl (Division of Immunopathology, Department of Pathophysiology and Allergy Research, Center of Pathophysiology, Infectiology and Immunology, Medical University of Vienna, Vienna, Austria) for helping with Bioplex 200 System (Bio-Rad). We thank the VBCF Protein Technologies facility (http://www.vbcf.ac.at) for providing reagents and advice for creation of CRISPR/Cas9 HuR-knockout cells. We thank Thierry Claudel (Division of Gastroenterology and Hepatology, Department of Medicine 3, Medical University of Vienna, Vienna, Austria) for primer design. We thank Walter Carbone (Novartis Institutes for Biomedical Research) for technical support. Some histological images were taken in cooperation with the Imaging Core Facility of the Medical University of Vienna.

Grant Support

The study was supported by the Federal Ministry of Economy, Family and Youth and the National Foundation for Research, Technology and Development, by the Austrian Science Fund (FWF P24121 to C. Gasche; P26127-B20 to O. Kuzyk and D. Berry), and by the Vienna Science and Technology Fund (WWTF project LS12-001 to A. Loy and D. Berry). In addition, P. Kovarik and C. Gasche received a joint research cluster grant (Oncology & Inflammation) from the University of Vienna and the Medical University of Vienna.

The costs of publication of this article were defrayed in part by the payment of page charges. This article must therefore be hereby marked *advertisement* in accordance with 18 U.S.C. Section 1734 solely to indicate this fact.

References

1. Meisner NC, Hackermuller J, Uhl V, Aszodi A, Jaritz M, Auer M. mRNA openers and closers: modulating AU-rich element-controlled mRNA stability by a molecular switch in mRNA secondary structure. Chembiochem. 2004; 5:1432–47. [PubMed: 15457527]
2. Wang J, Guo Y, Chu H, Guan Y, Bi J, Wang B. Multiple functions of the RNA-binding protein HuR in cancer progression, treatment responses and prognosis. Int J Mol Sci. 2013; 14:10015–41. [PubMed: 23665903]
3. Pascale A, Govoni S. The complex world of post-transcriptional mechanisms: is their deregulation a common link for diseases? Focus on ELAV-like RNA-binding proteins. Cell Mol Life Sci. 2012; 69:501–17. [PubMed: 21909784]
4. Denkert C, Koch I, von Keyserlingk N, Noske A, Niesporek S, Dietel M, et al. Expression of the ELAV-like protein HuR in human colon cancer: association with tumor stage and cyclooxygenase-2. Mod Pathol. 2006; 19:1261–9. [PubMed: 16799479]
5. Brosens LA, Keller JJ, Pohjola L, Haglund C, Morsink FH, Iacobuzio-Donahue C, et al. Increased expression of cytoplasmic HuR in familial adenomatous polyposis. Cancer BiolTher. 2008; 7:424–7.
6. Heinonen M, Bono P, Narko K, Chang SH, Lundin J, Joensuu H, et al. Cytoplasmic HuR expression is a prognostic factor in invasive ductal breast carcinoma. Cancer Res. 2005; 65:2157–61. [PubMed: 15781626]
7. Mrena J, Wiksten JP, Thiel A, Kokkola A, Pohjola L, Lundin J, et al. Cyclooxygenase-2 is an independent prognostic factor in gastric cancer and its expression is regulated by the messenger RNA stability factor HuR. Clin Cancer Res. 2005; 11:7362–8. [PubMed: 16243808]

8. Erkinheimo TL, Lassus H, Sivula A, Sengupta S, Furneaux H, Hla T, et al. Cytoplasmic HuR expression correlates with poor outcome and with cyclooxygenase 2 expression in serous ovarian carcinoma. Cancer Res. 2003; 63:7591–4. [PubMed: 14633672]
9. Nabors LB, Gillespie GY, Harkins L, King PH. HuR, a RNA stability factor, is expressed in malignant brain tumors and binds to adenine- and uridine-rich elements within the 3′ untranslated regions of cytokine and angiogenic factor mRNAs. Cancer Res. 2001; 61:2154–61. [PubMed: 11280780]
10. Koljonen V, Bohling T, Haglund C, Ristimaki A. Expression of HuR in Merkel cell carcinoma and in normal skin. J Cutan Pathol. 2008; 35:10–4. [PubMed: 18095988]
11. Danilin S, Sourbier C, Thomas L, Lindner V, Rothhut S, Dormoy V, et al. Role of the RNA-binding protein HuR in human renal cell carcinoma. Carcinogenesis. 2010; 31:1018–26. [PubMed: 20219773]
12. Lopez de Silanes I, Fan J, Yang X, Zonderman AB, Potapova O, Pizer ES, et al. Role of the RNA-binding protein HuR in colon carcinogenesis. Oncogene. 2003; 22:7146–54. [PubMed: 14562043]
13. Young LE, Sanduja S, Bemis-Standoli K, Pena EA, Price RL, Dixon DA. The mRNA binding proteins HuR and tristetraprolin regulate cyclooxygenase 2 expression during colon carcinogenesis. Gastroenterology. 2009; 136:1669–79. [PubMed: 19208339]
14. Kontoyiannis D, Pasparakis M, Pizarro TT, Cominelli F, Kollias G. Impaired on/off regulation of TNF biosynthesis in mice lacking TNF AU-rich elements: implications for joint and gut-associated immunopathologies. Immunity. 1999; 10:387–98. [PubMed: 10204494]
15. Taylor GA, Carballo E, Lee DM, Lai WS, Thompson MJ, Patel DD, et al. A pathogenetic role for TNF alpha in the syndrome of cachexia, arthritis, and autoimmunity resulting from tristetraprolin (TTP) deficiency. Immunity. 1996; 4:445–54. [PubMed: 8630730]
16. Ghosh M, Aguila HL, Michaud J, Ai Y, Wu MT, Hemmes A, et al. Essential role of the RNA-binding protein HuR in progenitor cell survival in mice. J Clin Invest. 2009; 119:3530–43. [PubMed: 19884656]
17. Katsanou V, Milatos S, Yiakouvaki A, Sgantzis N, Kotsoni A, Alexiou M, et al. The RNA-binding protein Elavl1/HuR is essential for placental branching morphogenesis and embryonic development. Mol Cell Biol. 2009; 29:2762–76. [PubMed: 19307312]
18. Giammanco A, Blanc V, Montenegro G, Klos C, Xie Y, Kennedy S, et al. Intestinal epithelial HuR modulates distinct pathways of proliferation and apoptosis and attenuates small intestinal and colonic tumor development. Cancer Res. 2014; 74:5322–35. [PubMed: 25085247]
19. Yiakouvaki A, Dimitriou M, Karakasiliotis I, Eftychi C, Theocharis S, Kontoyiannis DL. Myeloid cell expression of the RNA-binding protein HuR protects mice from pathologic inflammation and colorectal carcinogenesis. J Clin Invest. 2012; 122:48–61. [PubMed: 22201685]
20. Weiss WA, Taylor SS, Shokat KM. Recognizing and exploiting differences between RNAi and small-molecule inhibitors. Nat Chem Biol. 2007; 3:739–44. [PubMed: 18007642]
21. Meisner NC, Hintersteiner M, Mueller K, Bauer R, Seifert JM, Naegeli HU, et al. Identification and mechanistic characterization of low-molecular-weight inhibitors for HuR. Nat Chem Biol. 2007; 3:508–15. [PubMed: 17632515]
22. Lang M, Borgmann M, Oberhuber G, Evstatiev R, Jimenez K, Dammann KW, et al. Thymoquinone attenuates tumor growth in ApcMin mice by interference with Wnt-signaling. Mol Cancer. 2013; 12:41. [PubMed: 23668310]
23. Roig AI, Eskiocak U, Hight SK, Kim SB, Delgado O, Souza RF, et al. Immortalized epithelial cells derived from human colon biopsies express stem cell markers and differentiate in vitro. Gastroenterology. 2010; 138:1012–21. [PubMed: 19962984]
24. Sato T, Vries RG, Snippert HJ, van de Wetering M, Barker N, Stange DE, et al. Single Lgr5 stem cells build crypt-villus structures in vitro without a mesenchymal niche. Nature. 2009; 459:262–5. [PubMed: 19329995]
25. Griffiths RI, Whiteley AS, O'Donnell AG, Bailey MJ. Rapid method for coextraction of DNA and RNA from natural environments for analysis of ribosomal DNA- and rRNA-based microbial community composition. Appl Environ Microbiol. 2000; 66:5488–91. [PubMed: 11097934]

26. Klindworth A, Pruesse E, Schweer T, Peplies J, Quast C, Horn M, et al. Evaluation of general 16S ribosomal RNA gene PCR primers for classical and next-generation sequencing-based diversity studies. Nucleic Acids Res. 2013; 41:e1. [PubMed: 22933715]
27. Berry D, Ben Mahfoudh K, Wagner M, Loy A. Barcoded primers used in multiplex amplicon pyrosequencing bias amplification. Appl Environ Microbiol. 2011; 77:7846–9. [PubMed: 21890669]
28. Bokulich NA, Subramanian S, Faith JJ, Gevers D, Gordon JI, Knight R, et al. Quality-filtering vastly improves diversity estimates from Illumina amplicon sequencing. Nat Methods. 2013; 10:57–9. [PubMed: 23202435]
29. Wang Q, Garrity GM, Tiedje JM, Cole JR. Naive Bayesian classifier for rapid assignment of rRNA sequences into the new bacterial taxonomy. Appl Environ Microbiol. 2007; 73:5261–7. [PubMed: 17586664]
30. Edgar RC, Haas BJ, Clemente JC, Quince C, Knight R. UCHIME improves sensitivity and speed of chimera detection. Bioinformatics. 2011; 27:2194–200. [PubMed: 21700674]
31. Oksanen, JF., B, FG., Kindt, R., Legendre, P., O'Hara, RB., Simpson, GL., Solymos, P., et al. Vegan: community ecology package, R package version 1.17-4. 2010. Available from: http://cran.r-project.org/.
32. De Caceres M, Legendre P. Associations between species and groups of sites: indices and statistical inference. Ecology. 2009; 90:3566–74. [PubMed: 20120823]
33. Tatsuta, K., N, S., Takahashi, I. Preparation of MS-444 derivatives as immunosuppressive and anti-itching agents. Kyowa Hakko Kogyo Co., Ltd.; Japan: 1997. 98-JP265(9832750), 28. WO. 23-1-1998
34. von Roretz C, Lian XJ, Macri AM, Punjani N, Clair E, Drouin O, et al. Apoptotic-induced cleavage shifts HuR from being a promoter of survival to an activator of caspase-mediated apoptosis. Cell Death Differ. 2013; 20:154–68. [PubMed: 22955946]
35. Blanco FF, Preet R, Aguado A, Vishwakarma V, Stevens LE, Vyas A, et al. Impact of HuR inhibition by the small molecule MS-444 on colorectal cancer cell tumorigenesis. Oncotarget. 2016; 7:74043–58. [PubMed: 27677075]
36. Ahrens R, Waddell A, Seidu L, Blanchard C, Carey R, Forbes E, et al. Intestinal macrophage/epithelial cell-derived CCL11/eotaxin-1 mediates eosinophil recruitment and function in pediatric ulcerative colitis. J Immunol. 2008; 181:7390–9. [PubMed: 18981162]
37. You S, Ohmori M, Pena MM, Nassri B, Quiton J, Al-Assad ZA, et al. Developmental abnormalities in multiple proliferative tissues of Apc (Min/+) mice. Int J Exp Pathol. 2006; 87:227–36. [PubMed: 16709231]
38. Kim HH, Kuwano Y, Srikantan S, Lee EK, Martindale JL, Gorospe M. HuR recruits let-7/RISC to repress c-Myc expression. Genes Dev. 2009; 23:1743–8. [PubMed: 19574298]
39. Kakuguchi W, Kitamura T, Kuroshima T, Ishikawa M, Kitagawa Y, Totsuka Y, et al. HuR knockdown changes the oncogenic potential of oral cancer cells. Mol Cancer Res. 2010; 8:520–8. [PubMed: 20332213]
40. Atasoy U, Curry SL, Lopez de Silanes I, Shyu AB, Casolaro V, Gorospe M, et al. Regulation of eotaxin gene expression by TNF-alpha and IL-4 through mRNA stabilization: involvement of the RNA-binding protein HuR. J Immunol. 2003; 171:4369–78. [PubMed: 14530362]
41. Kim I, Kwak H, Lee HK, Hyun S, Jeong S. beta-Catenin recognizes a specific RNA motif in the cyclooxygenase-2 mRNA 3′-UTR and interacts with HuR in colon cancer cells. Nucleic Acids Res. 2012; 40:6863–72. [PubMed: 22544606]
42. Zucal C, D'Agostino V, Loffredo R, Mantelli B, Thongon Natthakan, Lal P, et al. Targeting the multifaceted HuR protein, benefits and caveats. Curr Drug Targets. 2015; 16:499–515. [PubMed: 25706256]
43. Nakanishi S, Chiba S, Yano H, Kawamoto I, Matsuda Y. MS-444, a new inhibitor of myosin light chain kinase from Micromonospora sp. KY7123. J Antibiot. 1995; 48:948–51. [PubMed: 7592060]
44. He WQ, Peng YJ, Zhang WC, Lv N, Tang J, Chen C, et al. Myosin light chain kinase is central to smooth muscle contraction and required for gastrointestinal motility in mice. Gastroenterology. 2008; 135:610–20. [PubMed: 18586037]

45. Swain SL. Interleukin 18: tipping the balance towards a T helper cell 1 response. J Exp Med. 2001; 194:F11–4. [PubMed: 11489958]

46. Gatault S, Delbeke M, Driss V, Sarazin A, Dendooven A, Kahn JE, et al. IL-18 Is involved in eosinophil-mediated tumoricidal activity against a colon carcinoma cell line by upregulating LFA-1 and ICAM-1. J Immunol. 2015; 195:2483–92. [PubMed: 26216891]

47. Chen YL, Huang YL, Lin NY, Chen HC, Chiu WC, Chang CJ. Differential regulation of ARE-mediated TNFalpha and IL-1beta mRNA stability by lipopolysaccharide in RAW264.7 cells. Biochem Biophys Res Commun. 2006; 346:160–8. [PubMed: 16759646]

48. Goldberg-Cohen I, Furneauxb H, Levy AP. A 40-bp RNA element that mediates stabilization of vascular endothelial growth factor mRNA by HuR. J Biol Chem. 2002; 277:13635–40. [PubMed: 11834731]

49. Pretlow TP, Keith EF, Cryar AK, Bartolucci AA, Pitts AM, Pretlow TG 2nd, et al. Eosinophil infiltration of human colonic carcinomas as a prognostic indicator. Cancer Res. 1983; 43:2997–3000. [PubMed: 6850611]

50. Young LE, Moore AE, Sokol L, Meisner-Kober N, Dixon DA. The mRNA stability factor HuR inhibits microRNA-16 targeting of COX-2. Mol Cancer Res. 2012; 10:167–80. [PubMed: 22049153]

51. Berry D, Stecher B, Schintlmeister A, Reichert J, Brugiroux S, Wild B, et al. Host-compound foraging by intestinal microbiota revealed by single-cell stable isotope probing. Proc Natl Acad Sci U S A. 2013; 110:4720–5. [PubMed: 23487774]

52. Elinav E, Strowig T, Kau AL, Henao-Mejia J, Thaiss CA, Booth CJ, et al. NLRP6 inflammasome regulates colonic microbial ecology and risk for colitis. Cell. 2011; 145:745–57. [PubMed: 21565393]

53. Lebedeva S, Jens M, Theil K, Schwanhausser B, Selbach M, Landthaler M, et al. Transcriptome-wide analysis of regulatory interactions of the RNA-binding protein HuR. Mol Cell. 2011; 43:340–52. [PubMed: 21723171]

54. Mukherjee N, Corcoran DL, Nusbaum JD, Reid DW, Georgiev S, Hafner M, et al. Integrative regulatory mapping indicates that the RNA-binding protein HuR couples pre-mRNA processing and mRNA stability. Mol Cell. 2011; 43:327–39. [PubMed: 21723170]

55. Lu YC, Chang SH, Hafner M, Li X, Tuschl T, Elemento O, et al. ELAVL1 modulates transcriptome-wide miRNA binding in murine macrophages. Cell Rep. 2014; 9:2330–43. [PubMed: 25533351]

Europe PMC Funders Author Manuscripts

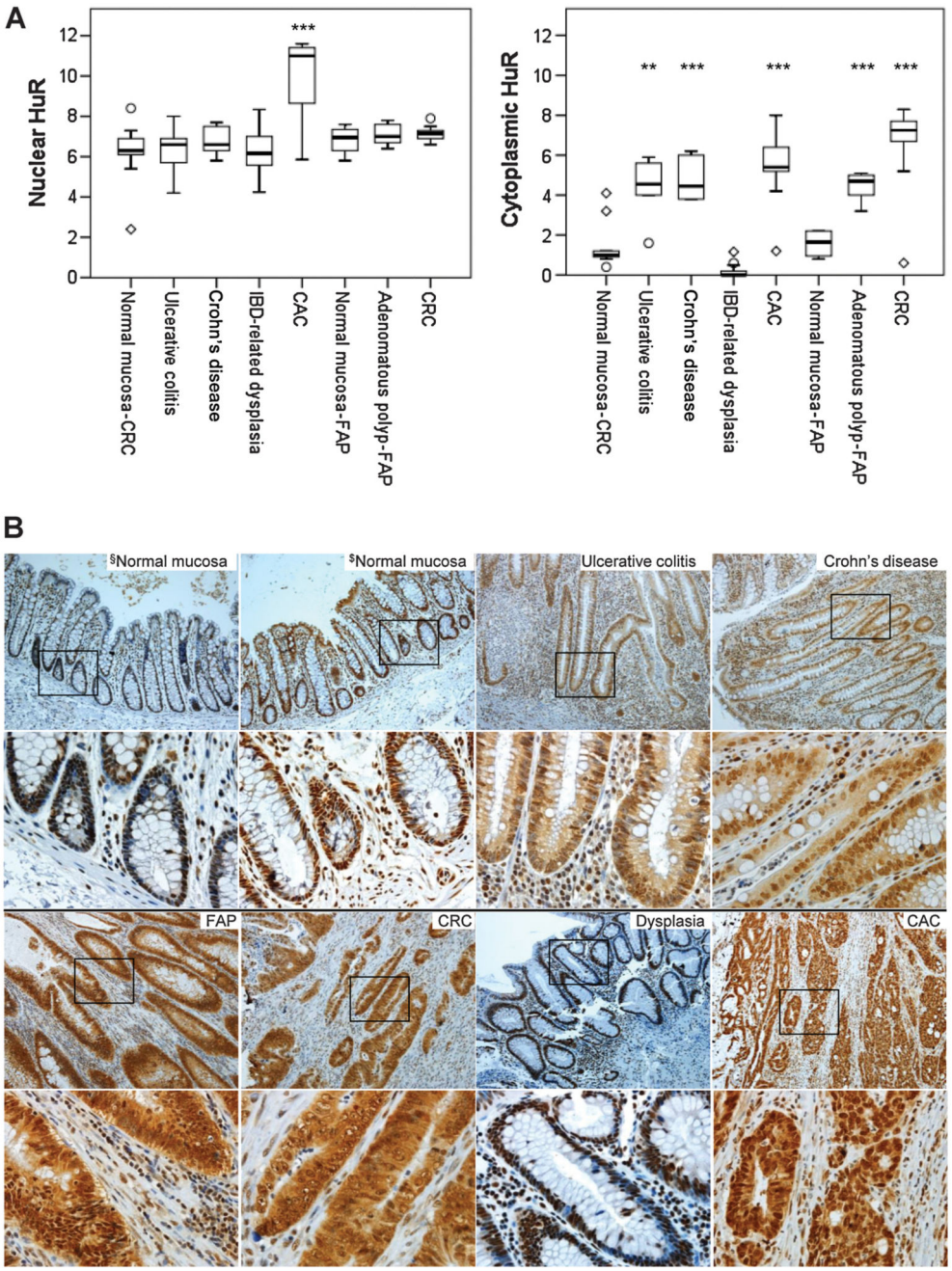

Figure 1.

HuR subcellular distribution in human intestinal disease. **A,** Nuclear and cytoplasmic HuR expression was scored in epithelial cells. In all large bowel tissue samples, HuR is highly expressed in the nucleus, with the highest expression in CAC samples. In ulcerative colitis, Crohn's disease, CAC, FAP-adenomas, and colorectal cancer (CRC) cytoplasmic HuR is significantly increased compared with normal mucosa. In IBD-related dysplasia, HuR cytoplasmic abundance is markedly decreased. **, $P < 0.01$; ***, $P < 0.001$; ANOVA, Tukey-HSD. **B,** Representative images of normal mucosa (§, from colorectal cancer patients;

[$], from FAP patients), ulcerative colitis, Crohn's disease, low-grade dysplasia, CAC, colorectal cancer, and FAP tissue samples stained for HuR shown at ×40 (top) and ×400 magnification (bottom).

Europe PMC Funders Author Manuscripts

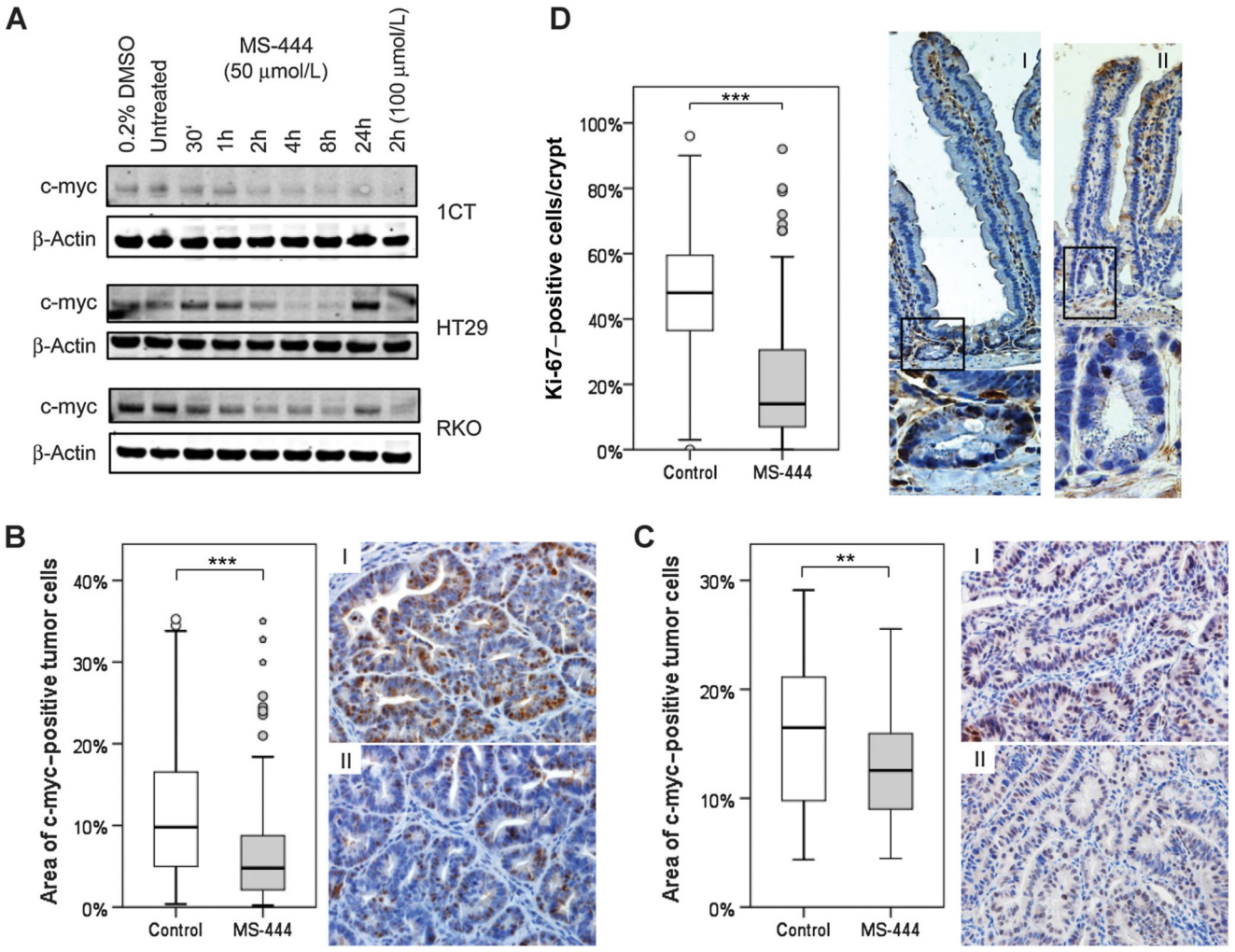

Figure 2.

Systemic HuR inhibition reduces c-myc protein expression and proliferation in both AOM/DSS and APC^{Min} mice. **A,** C-myc protein expression upon 50 µmol/L or 100 µmol/L MS-444 for up to 24 hours was analyzed in 1CT normal colonic epithelial cells and in the colorectal cancer cell lines HT29 and RKO by Western blot analysis. β-Actin was used as loading control. IHC analysis of c-myc expression in large bowel tumors of AOM/DSS mice (**B**), small intestinal tumors of APC^{Min} mice (**C**), and Ki-67 expression in small intestinal crypts of AOM/DSS mice (**D**) was performed. Representative images for c-myc (**B** and **C**) and Ki-67 (**D**) staining of control (**I**) and MS-444–treated (**II**) mice are shown; magnification, ×400. For c-myc, the area of positive tumor cells/FoV (AOM/DSS: $n_{control}$ = 158, $n_{MS\text{-}444\ treated}$ = 146; APC^{Min}: $n_{control}$ = 40, $n_{MS\text{-}444\ treated}$=50) was calculated. For Ki-67, the number of positive and total small intestinal crypt cells was counted ($n_{control}$ = 292, $n_{MS\text{-}444\ treated}$ = 240). Both c-myc and Ki-67–positive cells were significantly reduced upon MS-444 treatment. Statistical analysis, independent samples *t* test; **, $P < 0.01$; ***, $P < 0.001$.

Europe PMC Funders Author Manuscripts

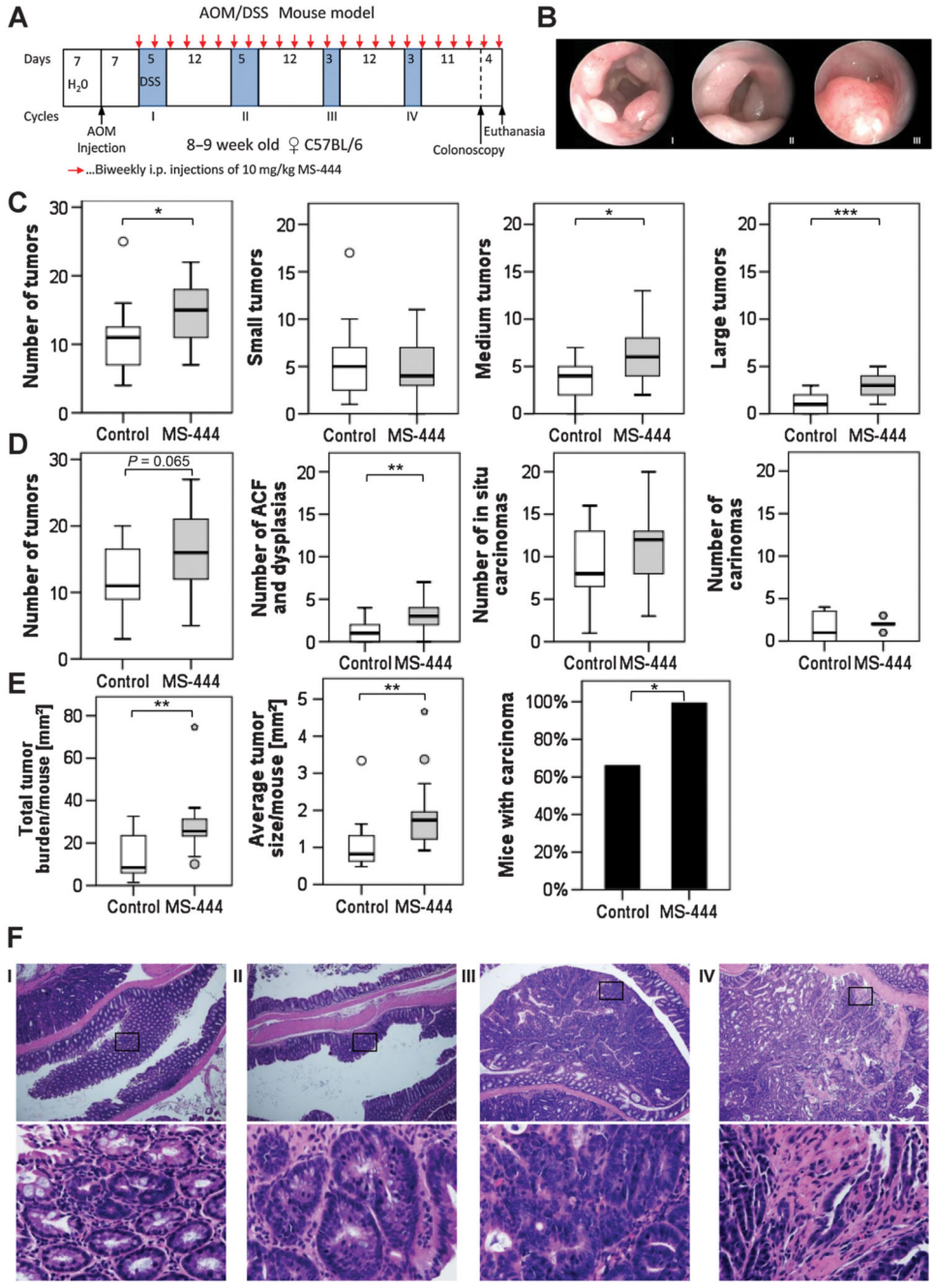

Figure 3.

HuR inhibition increases number and size of tumors in the AOM/DSS mouse. **A,** Schematic presentation of the treatment schedule in AOM/DSS mice. **B,** Tumors of different size, as detected by colonoscopy, are shown. **I,** small, <¼ of the colon circumference; **II,** medium, ¼ - ½ of the circumference; **III,** large, >½. **C,** The total number of distal tumors/mouse was significantly increased in the MS-444–treated group compared with control mice, as detected during colonoscopy (Mann–Whitney *U* test). No difference was found for small tumors; the number of medium and large tumors was significantly increased upon MS-444

Europe PMC Funders Author Manuscripts

treatment. **D,** Tumor multiplicity was increased in the MS-444–treated group compared with control mice, as the number of aberrant crypt foci (ACF) and dysplasias was significantly increased and a trend for increasing numbers of *in situ* and invasive carcinomas was found, as analyzed microscopically. **E,** The total tumor burden in mm^2/mouse nearly doubled upon MS-444 treatment. Similarly, the average tumor size/mouse increased from 1.1 (±0.7) to 1.9 (±1.1) mm^2. **F,** MS-444 treatment significantly increased the incidence of adenocarcinoma formation; $P = 0.044$; Fisher exact χ^2 test (two-sided). Exemplarily images for microadenomas/aberrant crypt foci (**I**), adenomas with low grade dysplasia (**II**), *in situ* carcinomas (**III**), and invasive adenocarcinomas (**IV**) are shown (top, ×40; bottom, ×400). *, $P < 0.05$; **, $P < 0.01$; ***, $P < 0.001$.

Europe PMC Funders Author Manuscripts

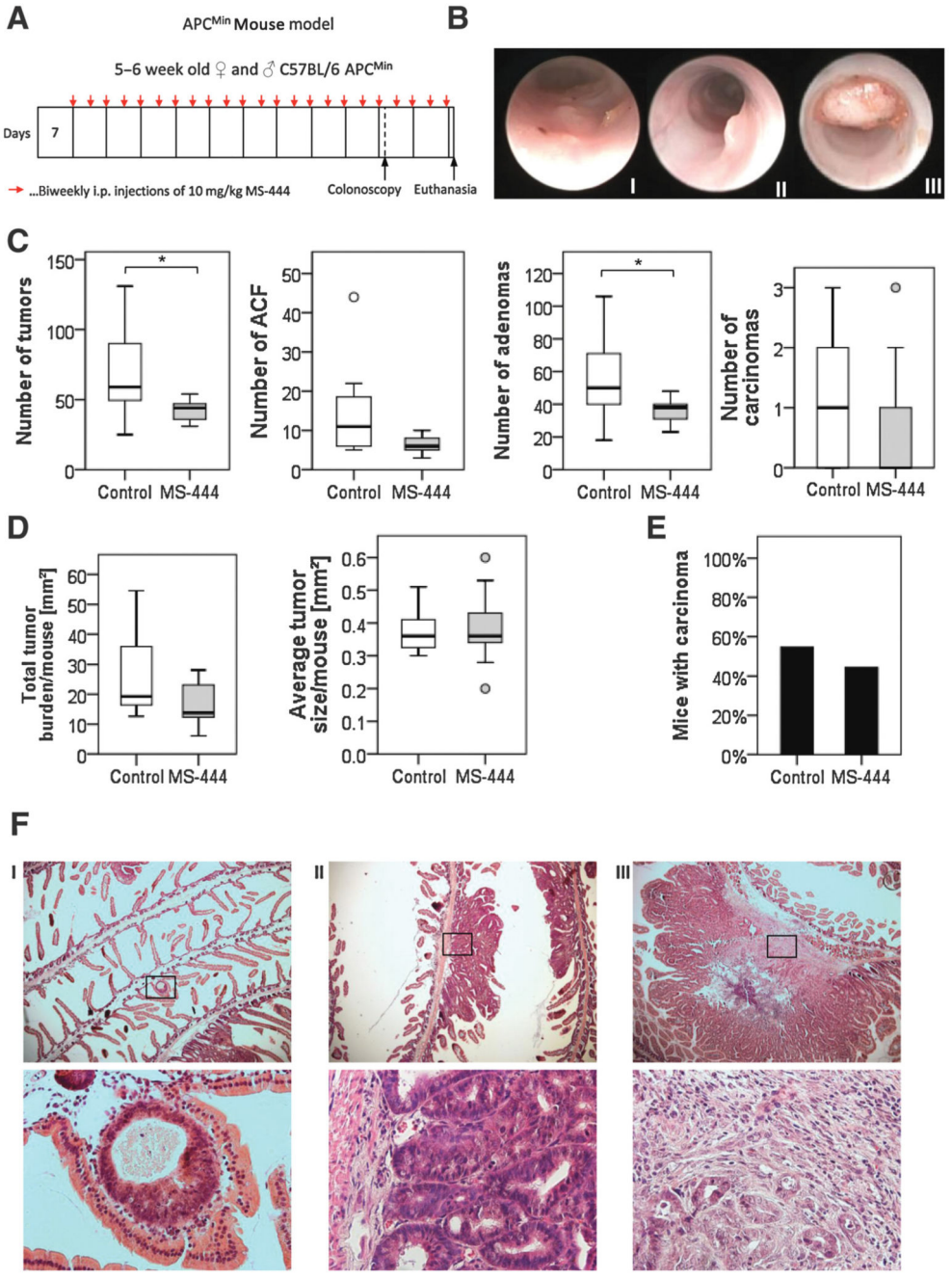

Figure 4.

HuR inhibition decreases tumor multiplicity but has no effect on tumor size in APC^{Min} mice. **A,** Schematic presentation of the treatment schedule in APC^{Min} mice. **B,** Representative colonoscopic images are shown. **I,** normal mucosa; **II,** small tumor, **III,** large tumor. **C,** The total number of tumors/mouse ($n_{control}$ = 11, n_{MS-444} = 9) decreased upon MS-444 compared with mock-treated mice (P = 0.03), with the most pronounced effect on adenoma regression (P = 0.03) and a trend for decreasing numbers of aberrant crypt foci (ACF) and carcinomas. The total tumor burden in mm^2/mouse declined upon MS-444

treatment ($P = 0.13$), but the average tumor size/mouse (**D**) and the adenocarcinoma incidence (**E**) were not altered upon MS-444 treatment. **F**, Exemplarily images of aberrant crypt foci (**I**), adenomas (**II**), and adenocarcinomas (**III**) are shown (top, 40×; bottom, ×400).

Europe PMC Funders Author Manuscripts

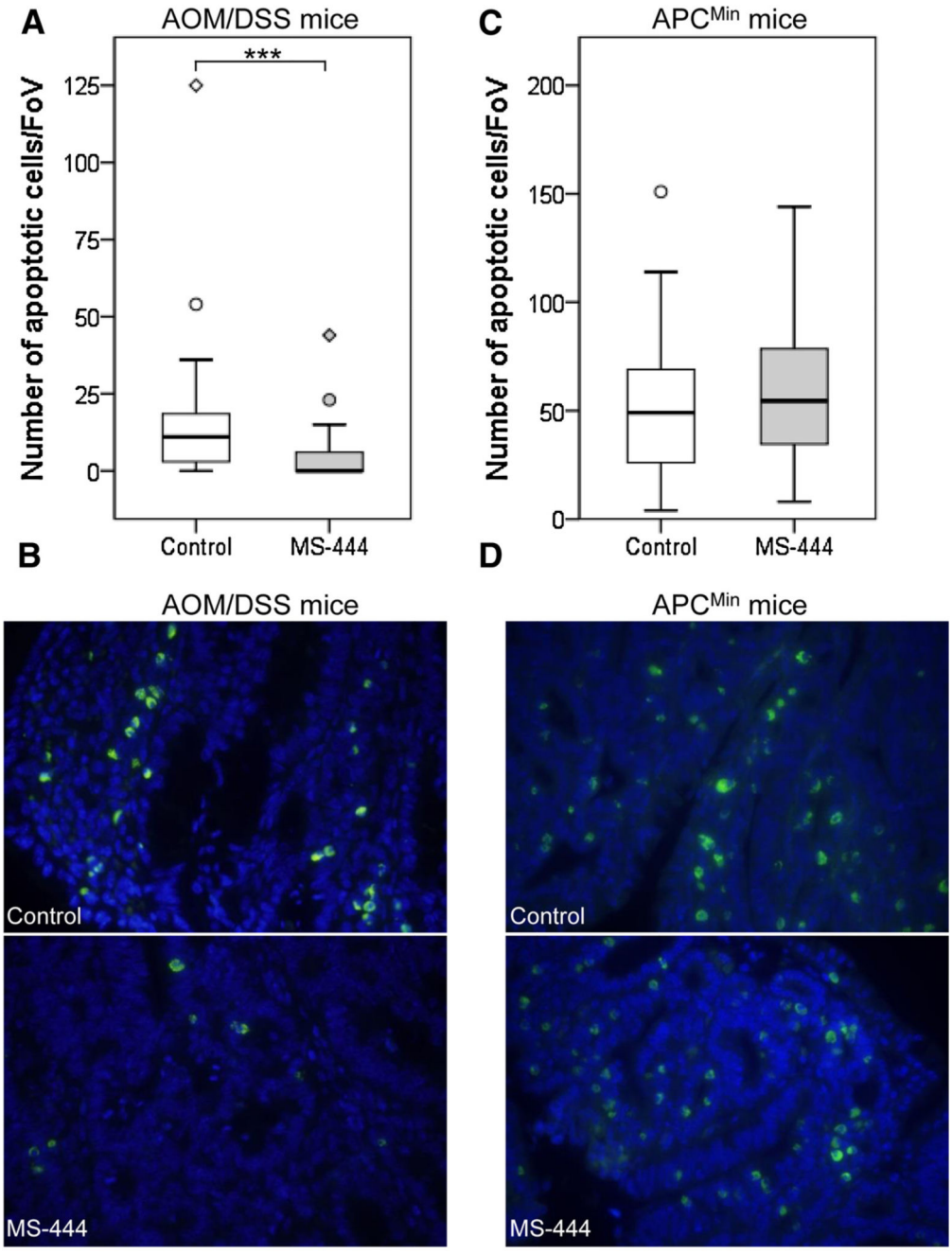

Figure 5.

HuR inhibition diminishes tumor cell apoptosis in the CAC mouse model but not in APC^{Min} mice. TUNEL staining was performed on intestinal sections of AOM/DSS–treated and APC^{Min} mice and apoptotic cells in 40 tumorigenic FoVs; each group was counted (40× objective). MS-444 administration decreased the number of apoptotic cells/tumor FoV in the large bowel of AOM/DSS mice (**A** and **B**) but not in small bowel tumors of APC^{Min} mice ($P = 0.333$) (**C** and **D**). Representative images of TUNEL-positive cells (green) of control (top)

and MS-444–treated (bottom) mice are shown. Nuclear counterstaining was performed with DAPI (blue). Mann–Whitney *U* test; ***, $P < 0.001$.

Europe PMC Funders Author Manuscripts

Europe PMC Funders Author Manuscripts

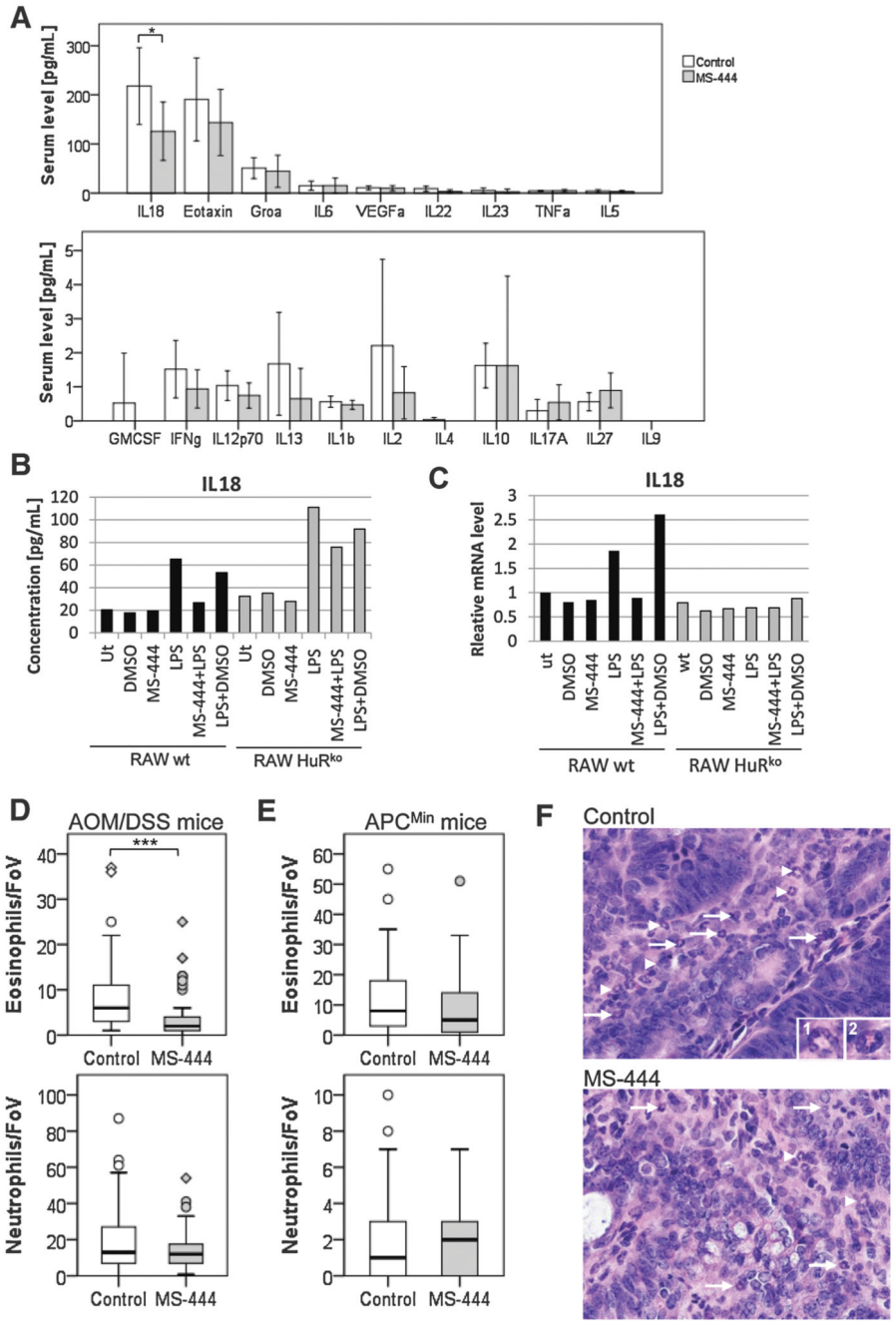

Figure 6.

Effect of MS-444 on immune cells. **A,** Serum cytokine expression in AOM/DSS–treated mice was analyzed using ProcartaPlex Multiplex Immunoassay. MS-444 significantly reduced IL18 serum levels ($P = 0.05$). A trend for reduced eotaxin ($P = 0.195$), IL22 ($P = 0.13$), and IL23 ($P = 0.15$) serum levels was found upon MS-444 treatment. Data are represented as mean ± SD ($n = 8$ mice per group, technical duplicates were performed). **B,** RAW 264.7 wt and HuR^{ko} (CRISPR/Cas9 HuR knockout) macrophages were treated with 10 ng/mL LPS and/or 50 μmol/L MS-444 for 4 hours. Untreated and DMSO-treated cells

were used as controls. IL18 secretion was assessed in supernatants of wt and HuR^{ko} RAWs using a Multiplex Immunoassay. **C,** Relative IL18 mRNA levels were calculated using qRT-PCR and 36b4 as endogenous control (technical duplicates were performed; data are representative of two independent experiments). **D** and **E,** Eosinophil and neutrophil infiltration into tumors was counted (60× objective; >60 FoVs were analyzed). Upon MS-444, the number of eosinophils was significantly reduced upon MS-444 in AOM/DSS–treated mice (**D**, top) but not in APC^{Min} mice (**E**, top). Neutrophils within tumors were not altered (**D** and **E**, bottom). **F,** Representative images of tumor-invading neutrophils (arrowhead, inset 1) and eosinophils (arrows, inset 2) in sham-treated (top) and MS-444–treated (bottom) AOM/DSS mice. *, $P \leq 0.05$; ***, $P < 0.001$.

Europe PMC Funders Author Manuscripts

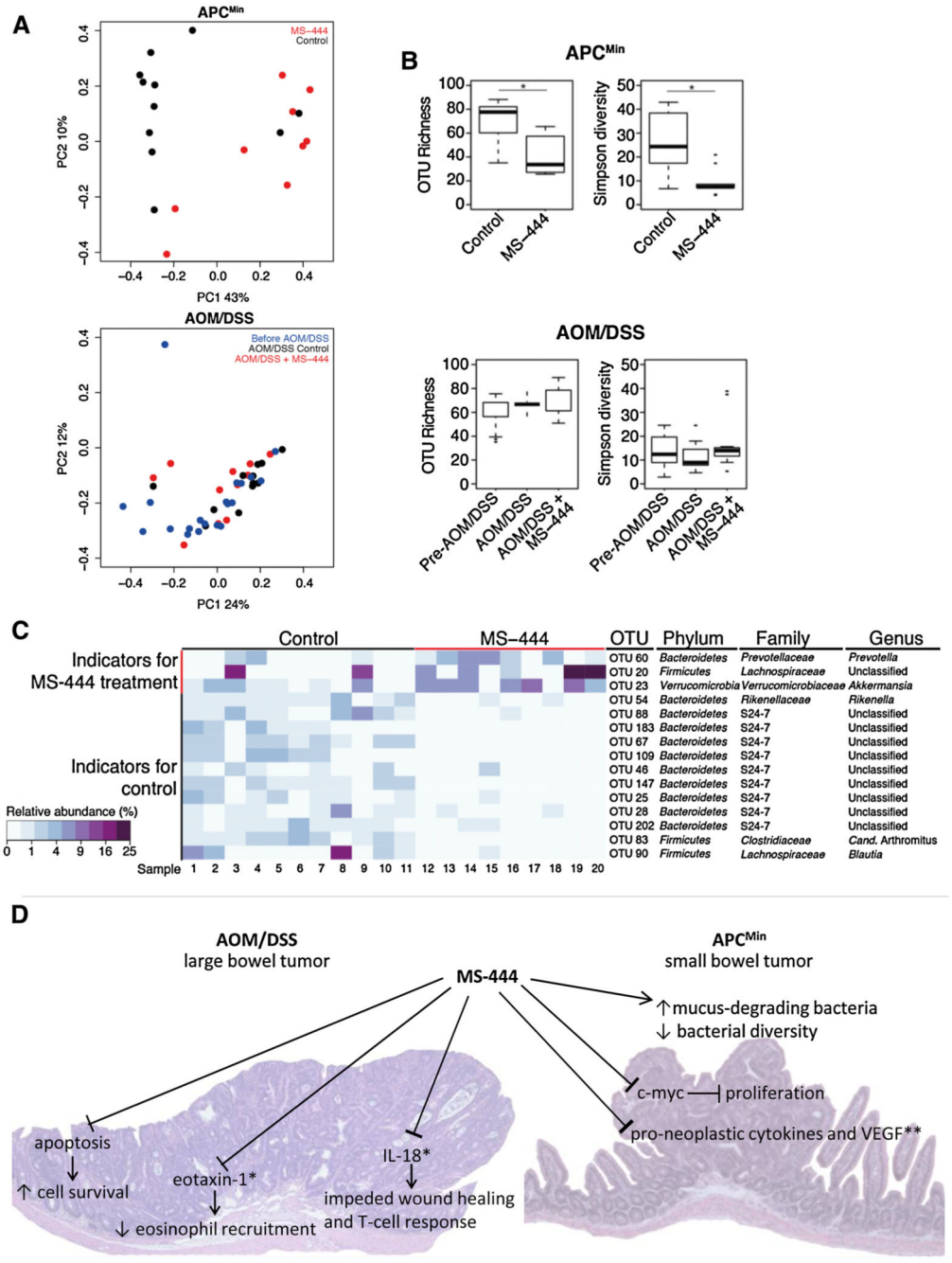

Figure 7.

Impact of MS-444 treatment on intestinal microbiota communities in APC^{Min} and AOM/DSS mice and MS-444 mode of action. **A,** A principal coordinates (PC) analysis, showing beta diversity, was performed using Bray–Curtis distances between samples. **B,** Alpha diversity of samples is shown by category. *, $P < 0.05$. **C,** Indicator OTUs for MS-444 treatment and controls in APC^{Min} mice. Heatmap coloring indicates the relative abundance of the OTU (%). The first three rows are indicators of treatment, and the others are all indicators for mock-treated controls. Summary figure of MS-444 activity. In AOM/DSS

Europe PMC Funders Author Manuscripts

mice, MS-444 reduces tumor cell apoptosis, which might lead to increased cell survival and increased tumor burden. **D,** Furthermore, eotaxin-1 levelswere reduced in sera (*) of AOM/DSS mice, reducing eosinophil recruitment. In addition, MS-444 reduced IL18 levels in sera, which might impede wound healing and T-cell response in response to DSS treatment. In APC^{Min} mice, MS-444 reduced tumor formation, most probably by inhibition of proliferation. As shown in small intestinal organoids (**), MS-444 reduced proneoplastic cytokines such as IL6 and TNFα and VEGF. In addition, MS-444 reduced bacterial diversity but increased mucus-degrading bacteria.